Capacity analysis of suction caissons used in catenary mooring systems

Analyse de la capacité des caissons à succion pour les systèmes d'ancrage à lignes caténaires

Helen P. Dunne, Chris M. Martin
Department of Engineering Science, University of Oxford, United Kingdom, helen.dunne@eng.ox.ac.uk

ABSTRACT: Suction caissons, also known as suction anchors, are commonly used as part of offshore mooring systems. Loading is applied to the caisson at the mooring attachment point, the location of which can be optimised for maximum holding capacity. In this paper, plane strain and three-dimensional finite element limit analyses are used to find the capacity of suction caissons that are loaded horizontally. Lower and upper bounds on the capacity are found, with adaptive mesh refinement used to reduce the bound gap in successive iterations of the solution. The influences of the caisson length-to-diameter aspect ratio, the soil strength profile, and the load location are considered. The soil is modelled as a rigid–plastic von Mises material with either constant undrained shear strength or strength that increases linearly with depth. Capacity charts showing the variation in caisson capacity with load location are presented, and failure mechanisms are discussed.

RÉSUMÉ: Les caissons à succion, aussi connus sous le nom d'ancrages à succion, font communément parti des systèmes d'ancrage utilisés offshore. Le chargement est exercé sur le caisson au point d'attache de l'ancrage et cet emplacement peut être optimisé de manière à obtenir la capacité de retenue maximum. Dans ce papier, les déformations planes et une analyse limite par la méthode des éléments finis sont utilisés afin de trouver la capacité d'un caisson a succion une fois chargé horizontalement. Les limites supérieures et inférieures de la capacité sont obtenues par le biais d'un raffinement du maillage adaptif, utilisé afin de réduire l'écart entre les deux limites lors des itérations successives de la solution. L'influence du rapport de forme du caisson, du profil de résistance du sol et de la direction du chargement sont considérés. Le sol est modélisé par un matériau de Von Mises rigide-plastique, ayant, soit une contrainte de cisaillement non-drainée constante, soit une contrainte augmentant linéairement avec la profondeur. Les graphiques de capacité montrant la variation de capacité d'un caisson en fonction de l'emplacement du point d'attache du chargement sont présentés et les mécanismes de rupture sont discutés.

KEYWORDS: limit analysis; finite element modelling; caissons; capacity analysis; offshore engineering

1 INTRODUCTION

Suction caissons used offshore have a thin, typically steel, embedded cylindrical wall and a circular top cap. They are widely used to anchor floating structures such as spars and FPSOs in areas where the seabed is composed of soft clay or silt, such that the undrained shear strength (s_u) is the governing soil parameter for preliminary design. When used as part of a catenary mooring system, suction caissons are subject to predominantly horizontal loading. The load (F in Figure 1) is transferred to the caisson at the mooring attachment point, which can be positioned at a depth, L_f, anywhere along the caisson length, L. It is generally accepted that the optimal load location for maximum holding capacity varies from $0.5L$ to $0.75L$ (Randolph and House 2002, Andersen et al. 2005). However, there remains minimal insight into how design parameters such as the caisson aspect ratio and soil strength profile affect the optimal load location.

Both two-dimensional (2D) and three-dimensional (3D) finite element analysis (FEA) have previously been applied to suction caisson holding capacity analysis (e.g. Zdravkovic et al. 2001). The results of an extensive industry-sponsored study were presented by Andersen et al. (2005), where capacities of suction caissons were predicted using limit equilibrium methods, plastic limit analysis methods, and FEA. It was found that 2D limit equilibrium methods, when used with 3D correction factors, gave a good prediction of 3D FEA results.

One disadvantage of using conventional displacement FEA is the lack of a direct error measure for the solution. By contrast, the use of combined lower bound (LB) and upper bound (UB) finite element limit analysis (FELA) provides a definitive bracket around the theoretical plastic capacity. The main limitation of FELA is the need to adopt a simple rigid–plastic soil constitutive model. However, this is essentially equivalent to a stiff elastic–perfectly plastic soil model of the sort often used in FEA predictions of caisson holding capacity.

This study considers three caisson length-to-diameter aspect ratios (L/D = 1, 2, 3) and two undrained shear strength profiles: a soil with uniform strength, and a soil with no mudline strength and a linear increase in strength with depth (Figure 1). It is assumed that negative excess pore pressures prevent tensile contact-breaking between the caisson and the soil, so the results are independent of soil unit weight. The available shear strength on the caisson/soil interface is modelled as a roughness factor times the strength of the adjacent soil (αs_u, with α taken as 0.5). Horizontal live loading is applied to the caisson at intervals of $0.1L$ along the caisson length. Plane strain and 3D FELA are used to produce capacity charts showing the effect of load location on the holding capacity. Typical failure mechanisms are also presented and discussed.

1.1 *Finite element limit analysis*

All analyses were performed using OxLim, a FELA program based on methods developed by Makrodimopoulos and Martin (2006, 2007). OxLim has been used extensively for the analysis of bearing capacity problems in plane strain (e.g. Martin and White 2012, Mana et al. 2013, Dunne et al. 2015) and more recently for capacity analysis of 3D shallow foundations

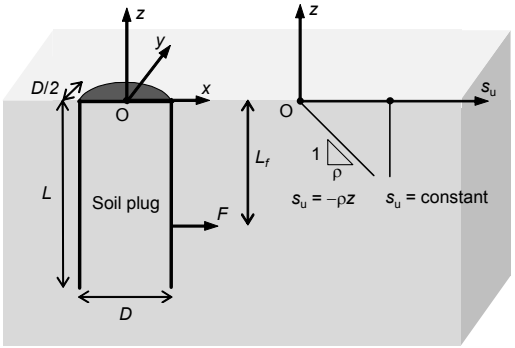

Figure 1. Notation and sign conventions used in 3D FELA. The cross-section along $y = 0$ is used in plane strain FELA.

(Martin et al. 2015, Dunne and Martin 2016).

To use OxLim, the soil domain is first discretised into a mesh of triangles for a plane strain analysis or tetrahedra for a 3D analysis. Two separate constrained optimisation problems are then set up by the program to provide LB and UB solutions for the collapse load multiplier. The average of the bounds, $(LB + UB)/2$, is used as the best estimate solution, and the associated bracketing error is $\pm (UB - LB)/(UB + LB)$. For the plane strain analyses in this paper, unstructured meshes were generated using Triangle (Shewchuk 2002). Automated adaptive mesh refinement was used to reduce the bracketing error over successive iterations to ±1% or better. A similar approach was taken for the 3D analyses, but with mesh generation performed using TetGen (Si 2013) and a less stringent bracketing target. The largest bracketing error for the present 3D analyses was ±6.5%.

The undrained soil was modelled as a rigid–plastic material obeying the von Mises failure criterion, which allowed the LB and UB analyses to be cast as standard second-order cone programming problems and solved efficiently using specialised optimisation software (MOSEK ApS 2014). The von Mises yield strength in pure shear, k, was equated with the Tresca shear strength, s_u, such that the two criteria were matched for deformation in plane strain. As discussed above, the two strength profiles considered were uniform (s_u = constant) and normally consolidated ($s_u = -\rho z$). In the latter case it was convenient to normalise the holding capacity with respect to the average shear strength ($s_{u,av}$) at $z = -L/2$ (Figure 1). The capacities of caissons modelled in plane strain were extrapolated for a slice of thickness D in the y-direction.

In the 3D FELA model the plane of symmetry along $y = 0$ was exploited, and the curved caisson wall was approximated with 45 linear facets inscribing a half cylinder. The thickness of the caisson wall was modelled as $0.01D$. It was ensured that the extent of the modelled soil domain was sufficiently large to contain the failure mechanism comfortably, and the dimensions were varied depending on the caisson aspect ratio (Figure 2).

2 RESULTS

Normalised capacities of caissons when loaded horizontally at various points along the caisson length are shown in Figure 3(a) for uniform soil and Figure 3(b) for normally consolidated soil. The optimal depth of the attachment point (to the nearest $0.1L$) obtained using 3D FELA is referred to as L_{opt}. The solid lines in Figure 3 indicate that caissons in uniform soil have $L_{opt} = 0.6L$, irrespective of the aspect ratio L/D, whereas for caissons in normally consolidated soil the optimal load location is deeper, at $L_{opt} = 0.7L$.

The capacity of a caisson reduces rapidly the further it is loaded away from L_{opt}. The rate of reduction in capacity is more severe in normally consolidated soil than in uniform soil. The maximum capacity of a caisson with $L/D = 3$ embedded in soil with $s_u = -\rho z$ is $10.1DLs_{u,av}$. When the same caisson is loaded just $0.1L$ above the optimal load location L_{opt}, the capacity reduces by 24% to $7.7DLs_{u,av}$ (see Figure 3(b)).

The capacities obtained using plane strain FELA are shown as dashed lines in Figure 3. For a caisson with $L/D = 1$, loaded at the mudline ($L_f/L = 0$), the plane strain capacity is only 13% lower than the 3D capacity in uniform soil, and 10% lower in normally consolidated soil. However, as L_f increases from zero to L_{opt} the difference between the plane strain and 3D capacities increases. In normally consolidated soil (Figure 3(b)), the trend of the plane strain capacities as the load location is varied matches the trend of the 3D capacities reasonably well, while in uniform soil (Figure 3(a)), the plane strain analysis predicts an optimal load location that is marginally higher (by $0.1L$) than that from the 3D analysis.

For both soil strength profiles, particularly when $L/D > 1$, there are large differences between the simplified plane strain and true 3D capacities. For example, a caisson with $L/D = 3$ in uniform soil has a maximum plane strain capacity that is less than half the maximum 3D capacity.

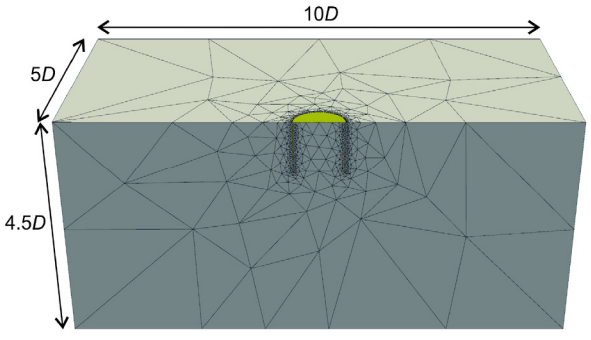

Figure 2. Initial 3D FELA mesh for caisson with $L/D = 1$. Symmetry exploited in the plane $y = 0$.

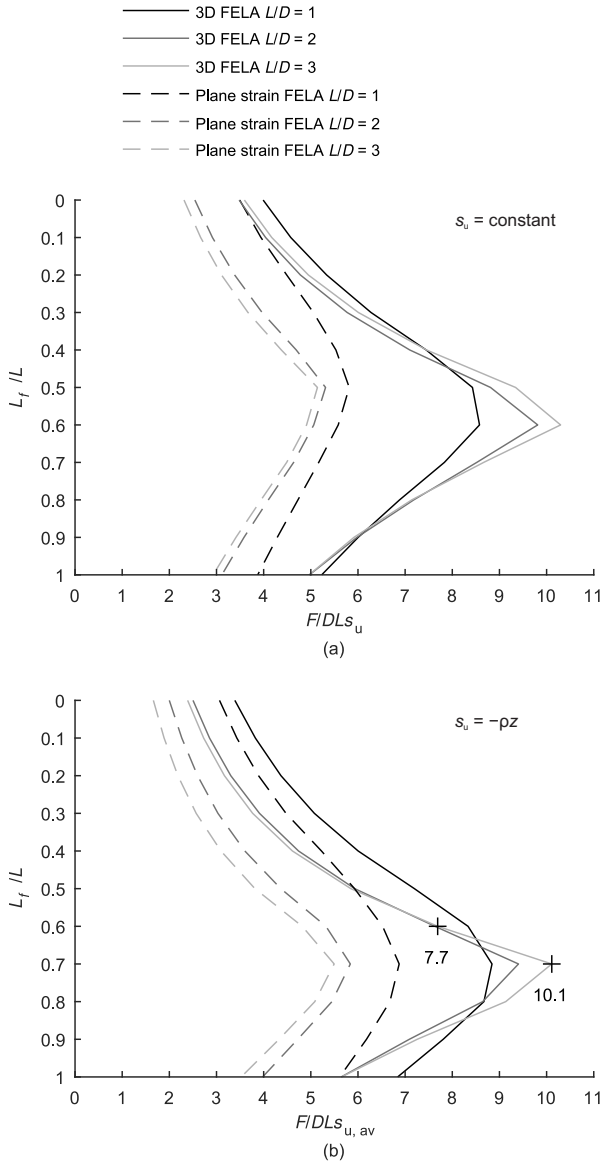

Figure 3. Normalised capacities of caissons modelled in 3D and plane strain when loaded at intervals of $0.1L$ along the caisson length: (a) s_u = constant; (b) $s_u = -\rho z$.

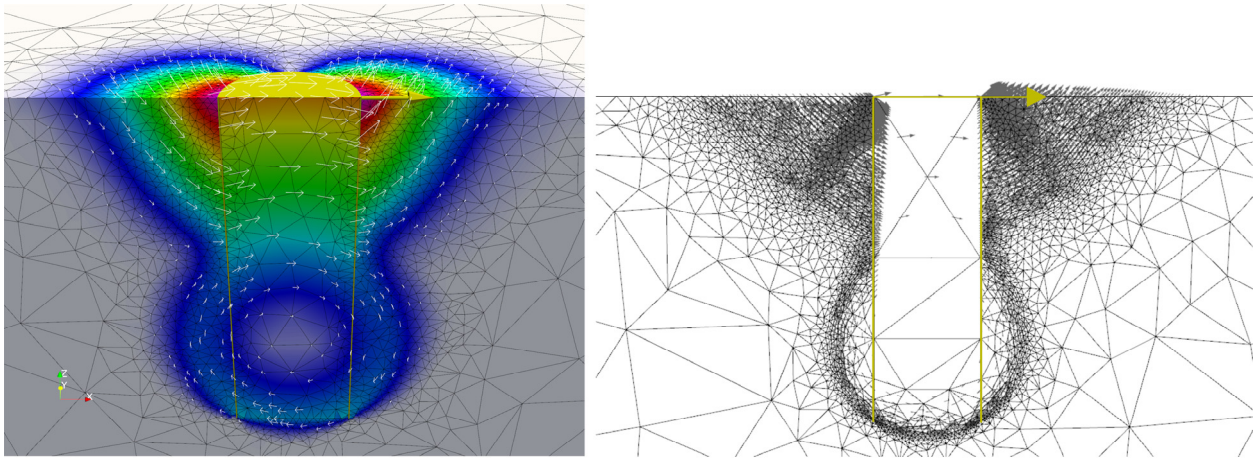

(a) (b)

Figure 4. Failure mechanisms of a caisson with $L/D = 3$ when loaded at the mudline ($L_f/L = 0$), s_u = constant. Shading and vectors show UB velocity magnitudes and directions: (a) 3D FELA; (b) plane strain FELA.

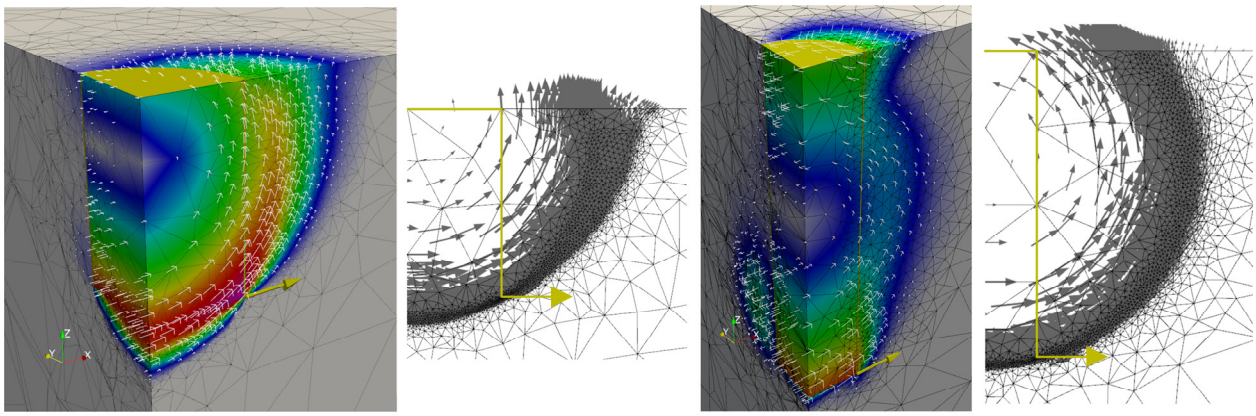

(a) (b) (c) (d)

Figure 5. Failure mechanisms of caissons when loaded at the caisson base ($L_f/L = 1$), s_u = constant. Cut-away view showing domain $x \geq 0$. Shading and vectors show UB velocity magnitudes and directions: (a) $L/D = 1$, 3D FELA; (b) $L/D = 1$, plane strain FELA; (c) $L/D = 3$, 3D FELA; (d) $L/D = 3$, plane strain FELA.

The plane strain and 3D capacities compare most favourably when the caisson is loaded at the mudline, and least favourably when it is loaded at L_{opt}. The 3D failure mechanism for a caisson with $L/D = 3$ in uniform soil, loaded at the mudline, is shown in Figure 4(a). The caisson rotates clockwise at failure, with active and passive wedges of soil developing near the mudline. Below these, a circular flow pattern is visible. The 3D mechanism involves minimal lateral soil flow around the caisson, and consequently the plane strain mechanism in Figure 4(b) closely resembles the 3D mechanism in the plane $y = 0$.

A caisson loaded below L_{opt} rotates counter-clockwise at failure, though the failure mechanism in the soil depends on the caisson aspect ratio. The 3D mechanism for a caisson with $L/D = 1$ in uniform soil, loaded at its base, is shown in Figure 5(a). In the plane $y = 0$ a circular flow pattern is visible, and there is negligible lateral soil flow around the caisson. The corresponding plane strain mechanism (Figure 5(b)) is similar to the 3D mechanism in the plane $y = 0$. The 3D mechanism when $L/D = 3$ is shown in Figure 5(c). This mechanism is more complex than the one in Figure 5(a), involving additional deforming regions near the mudline and towards the base of the caisson. At the mudline, active and passive wedges of soil are mobilised. Below the centre of rotation, the predominant mechanism is lateral soil flow around the caisson. These features are not identifiable in the failure mechanism from the corresponding plane strain analysis (Figure 5(d)).

When a caisson is loaded at the optimal location L_{opt}, the failure mechanism is again dependent on the aspect ratio. When $L/D = 1$ there is negligible lateral soil flow around the caisson. When $L/D > 1$ the 3D mechanism is dominated by lateral soil flow around the caisson at depths below $z = -L/2$ (Figure 6(a)). Clearly this behaviour cannot be captured by the corresponding plane strain analysis (Figure 6(b)).

As the caisson aspect ratio L/D increases, the maximum normalised 3D capacity increases, but the maximum normalised plane stain capacity decreases (Figure 3). Upon consideration of the failure mechanisms, the increase in normalised capacity with increasing aspect ratio in a 3D analysis can be attributed to increased lateral soil flow around the caisson. In a plane strain analysis, lateral soil flow around the caisson is not possible; increasing the caisson aspect ratio therefore results in a lower normalised capacity, as the relative contribution of base shear to the overall capacity is reduced.

The capacity of horizontally loaded caissons is highest when, at failure, the caisson undergoes translation without any rotation. Randolph and Houlsby (1984) used the method of characteristics to find LB and UB solutions for the plastic capacity of a circular pile section translating in cohesive soil. The UB solution was improved by Martin and Randolph (2006) for piles with $\alpha < 1$. Figure 7 shows the maximum normalised capacities of horizontally loaded caissons from 3D FELA (LB, UB and average) as well as the UB capacity of a translating pile section with $\alpha = 0.5$ (Martin and Randolph, 2006). As the caisson aspect ratio increases, the maximum normalised capacity (obtained for loading applied at L_{opt}) approaches the theoretical limit. This increase in capacity as L/D increases corresponds to a failure mechanism that becomes increasingly dominated by lateral soil flow around the caisson.

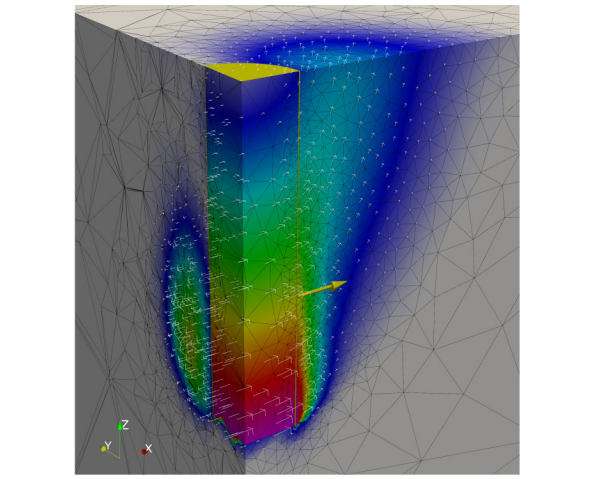

(a)

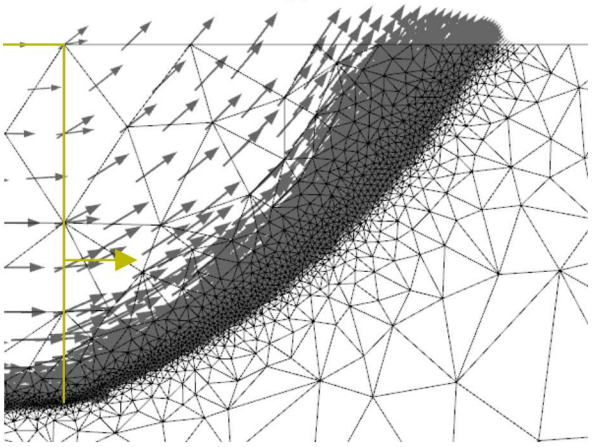

(b)

Figure 6. Failure mechanisms of a caisson with $L/D = 3$ when loaded at $L_{opt} = 0.6L$, s_u = constant. Cut-away view showing domain $x \geq 0$. Shading and vectors show UB velocity magnitudes and directions: (a) 3D FELA; (b) plane strain FELA.

3 CONCLUSIONS

This study has focused on the ultimate limit state analysis of offshore suction caissons in clay, where undrained capacity is critical for design. Rigorous 3D limit load analyses were carried out using FELA, varying the caisson length-to-diameter aspect ratio, the soil strength profile and the location of the mooring attachment point.

It has been shown that for a horizontally loaded caisson, the optimal loading location is independent of aspect ratio over the range considered here ($L/D = 1$ to 3). In uniform soil, the optimal location (to the nearest $0.1L$) is $0.6L$ from the mudline, and in normally consolidated soil, $0.7L$ from the mudline.

The effectiveness of using plane strain analyses to identify 3D caisson failure mechanisms has also been explored. It was found that in many instances, in particular when $L/D > 1$ and when loading is applied away from the mudline, the failure mechanism obtained from a plane strain analysis is not representative of the 3D failure mechanism, where soil is able to flow laterally around the caisson at depth.

It has been shown that as L/D increases, the maximum normalised capacity of a caisson approaches that of a circular pile section translating horizontally. When $L/D = 3$, the maximum normalised capacity is close to that of a pile section translating horizontally (Figure 7), which allows for easy approximation of the optimal capacity of caissons with $L/D > 3$.

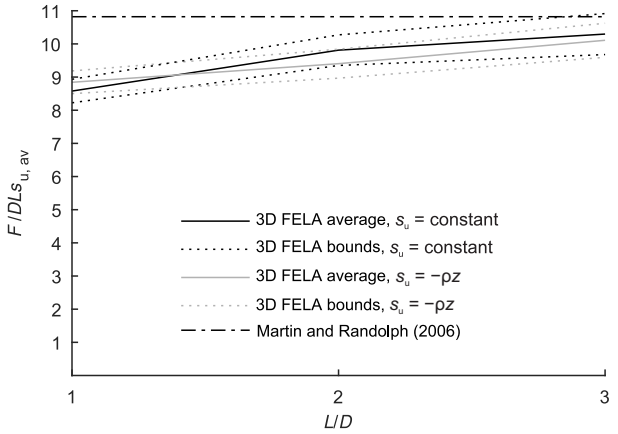

Figure 7: Maximum normalised capacities of caissons with roughness factor $\alpha = 0.5$.

4 ACKNOWLEDGEMENTS

The first author is grateful for doctoral studentship funding received from Subsea 7.

5 REFERENCES

Andersen K.H., Murff J.D., Randolph M.F., Clukey E.C., Erbrich C.T., Jostad H.P., Hansen B., Aubeny C., Sharma P., and Supachawarote C. 2005. Suction anchors for deepwater applications. *Proc. 1st Int. Symp. on Frontiers in Offshore Geotech., Perth* 1, 3-30.

Dunne H.P. and Martin C.M. 2016. Capacity of rectangular mudmat foundations under combined loading. *Géotechnique*, published online 03/10/2016 (doi: 10.1680/jgeot.16.P.079).

Dunne H.P., Martin C.M., Muir L., Brown N. and Wallerand R. 2015. Undrained bearing capacity of skirted mudmats on inclined seabeds. *Proc. 3rd Int. Symp. on Frontiers in Offshore Geotech., Oslo* 2, 783-788.

Mana D.S.K., Gourvenec S. and Martin C.M. 2013. Critical skirt spacing for shallow foundations under general loading. *J. Geotech. Geoenviron. Engng* 139(9), 1554-1566.

Makrodimopoulos A. and Martin C.M. 2006. Lower bound limit analysis of cohesive-frictional materials using second-order cone programming. *Int. J. Num. Meth. Engng* 66(4), 604-634.

Makrodimopoulos A. and Martin C.M. 2007. Upper bound limit analysis using simplex strain elements and second-order cone programming. *Int. J. Num. Anal. Meth. Geomech.* 31(6), 835-865.

Martin C.M. and Randolph M.F. 2006. Upper bound analysis of lateral pile capacity in cohesive soil. *Géotechnique* 56(2), 141-145.

Martin C.M. and White D.J. 2012. Limit analysis of the undrained bearing capacity of offshore pipelines. *Géotechnique* 62(9), 847-863.

Martin C.M., Dunne H.P., Wallerand R. and Brown N. 2015. Three-dimensional limit analysis of rectangular mudmat foundations. *Proc. 3rd Int. Symp. on Frontiers in Offshore Geotech., Oslo* 2, 789-794.

Randolph M.F. and Houlsby G.T. 1984. The limiting pressure on a circular pile loaded laterally in cohesive soil. *Géotechnique* 34(4), 613-623.

Randolph M.F. and House A.R. 2002. Analysis of suction caisson capacity in clay. *Proc. Offshore Technology Conf., Houston*, Paper OTC 14236.

MOSEK ApS 2014. *The MOSEK C Optimizer API manual*, version 7.1. See http://www.mosek.com.

Shewchuk J.R. 2002. Delaunay refinement algorithms for triangular mesh generation. *Comput. Geom.* 22(1-3), 21-74.

Si H. 2013. *TetGen User's Manual*, version 1.5. See http://wias-berlin.de/software/tetgen/1.5/doc/manual/index.html.

Zdravkovic L., Potts D.M. and Jardine R.J. 2001. A parametric study of the pull-out capacity of bucket foundations in soft clay. *Géotechnique* 51(1), 55-67.